THE JOURNAL OF PHYSICAL CHEMISTRY C
A JOURNAL OF THE AMERICAN CHEMICAL SOCIETY

pubs.acs.org/JPCC
Article

Flexible Hydrogel Electrolytes for Organic Batteries with High Cyclability

Lada Elbinger, Erik Schröter, Philip Zimmer, Christian Friebe, Markus Osenberg, Ingo Manke, and Ulrich S. Schubert*

Cite This: J. Phys. Chem. C 2024, 128, 11465−11476

Read Online

ACCESS | Metrics & More | Article Recommendations | Supporting Information

ABSTRACT: The growing interest in organic batteries for the sustainable storage of energy is giving rise not only to new polymeric active materials for batteries but also to new electrolyte systems. Water-based electrolytes are particularly interesting due to the sheer abundance of water on our planet and its cost-effective, sustainable, nonhazardous, and nonflammable nature. To further increase the safety of aqueous battery cells, various strategies have been pursued, of which the use of solid and gel electrolytes is one of the most prominent. Here, we present an efficient approach for a new environmentally friendly hydrogel electrolyte with high ionic conductivity (20 ± 1 mS cm^{-1} at room temperature) and medium ionic conductivity at low temperature (5.3 ± 0.3 mS cm^{-1} at −20 °C) based on commercially available monomers and a zinc salt compatible with the redox chemistry of the 2,2,6,6-tetramethylpiperidine-*N*-oxyl radical in a semiorganic battery setup. We investigate its battery cycling behavior and compare its performance with that of a previously analyzed analog that does not contain a hydrogel.

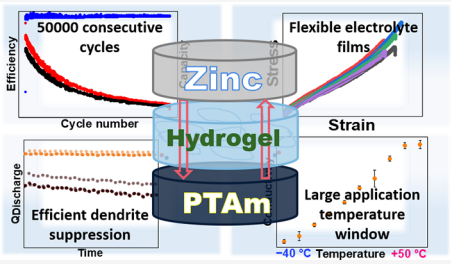

INTRODUCTION

Safe and efficient electrochemical storage devices have long been sought.[1,2] Lithium-ion batteries (LIBs) are currently the industry standard for small- and large-scale energy storage, offering high energy efficiency, high energy density, high cycling capability, and long shelf life.[3] However, LIBs also have drawbacks, such as their sensitivity to temperature, limitations in terms of production, and the often toxic and volatile electrolytes used.[4]

Today, the focus is not only on the capacity and longevity of electronic devices but also on their flexibility, leading to the demand for flexible energy storage systems, which require not only flexible electrodes but also a suitable electrolyte. The choice of electrolyte for such systems is critical because it is responsible for ion transport during electrochemical reactions and charge equilibration and defines the electrochemical stability window (ESW) of the system.[5,6] The most commonly used type is the electrolyte-soaked glass fiber separator, which distributes the electrolyte between the anode and the cathode.[7] However, liquid electrolytes are not the best choice for batteries for a number of reasons. First, liquids can leak if the cell is damaged, which can pose a safety risk to the device. More volatile electrolytes can partially evaporate, which has the effect of increasing salt concentration and electrical resistance in the system.[8] In addition, winter temperatures often drop below 0 °C, where liquid aqueous electrolytes tend to freeze despite the ion-supporting electrolyte additives. This severely limits the mobility of ions in the electrolyte and the wettability of the electrode. This results in deterioration of the electrode−electrolyte interface.[9] There are two preferred ways of solving this problem, namely, (a) using a highly concentrated salt solution or (b) using antifreeze agents (ethylene glycol, glycerine, etc.).[10,11]

In addition to the electrolyte, the choice of separator represents a critical factor. Unsuitable separator materials can result in poor separator−electrolyte contact interfaces or low ion permeabilities, leading to limited ion conductivities. Furthermore, a mechanically unstable separator may cause short circuits between electrode surfaces.[12] To address these challenges, hydrogel electrolytes are under investigation and represent an excellent alternative to commonly used electrolyte−separator combinations. They combine the typical advantages of water, i.e., high ion conductivities, with effective electrode separation.[13,14] As a result, there is growing interest in the use of polymer hydrogels as electrolytes and separators for batteries. Typical hydrogels consist of elastic polymer chains that are chemically or physically cross-linked to form interstitial spaces in a polymer network that is filled with the aqueous electrolyte.[15] The three-dimensional (3D) polymer network in the hydrogel structure can enhance ionic conductivity and provide excellent mechanical stability.[16]

Received: January 30, 2024
Revised: May 21, 2024
Accepted: May 22, 2024
Published: July 8, 2024

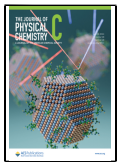

Deng et al. demonstrated that hydrogel electrolytes can also increase the capacity and cycle life of the battery and improve the energy density. Due to the high salt concentration in the gel, the voltage windows expand and can also be used at a wider range of operating temperatures.[17]

In this work, we focus on the development of a flexible polymer hydrogel electrolyte compatible with organic electrodes. There are already several suitable polymer matrices that have been studied in recent years, namely, poly(vinyl alcohol) (PVA), poly(ethylene glycol) (PEG), polyacrylamide (PAM), gelatin, xanthan gum, and others.[18−22] We have chosen a copolymer of poly(ethylene glycol) methyl ether acrylate (PEGMEA) and poly(acrylnitrile) (PAN) due to the high degree of hydrophilicity, good solubility in water, and the low toxicity of the resultant polymers. Additionally, the PEG chains are flexible, which has a direct influence on the mechanical properties of the hydrogel.[23]

Poly(TEMPO methacrylamide) (PTMAm), which was investigated and presented earlier by our group, was chosen as the cathode material. It features the 2,2,6,6-tetramethylpiperidinyl-*N*-oxyl (TEMPO) moiety providing a reversible one-electron redox reaction with fast kinetics (Scheme 1).[24]

Scheme 1. Schematic Representation of the TEMPO-Based Redox Processes upon Charging/Discharging

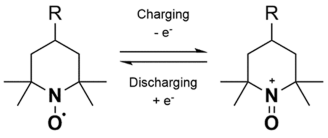

An oversized zinc counter electrode was used due to its high hydrophilicity, excellent stability, high capacity retention (>99% after 1000 cycles at 5C), straightforward, and large-scale availability.[25] In this work, two systems of the PTMAm cathode and zinc anode with aqueous and hydrogel electrolytes were compared and characterized.

EXPERIMENTAL METHODS

A description of the materials and the equipment as well as nuclear magnetic resonance (NMR) and infrared (IR) spectra can be found in the Supporting Information.

General Procedure for Hydrogel Electrolyte Manufacturing. The PEGMEA-(PEG-DA)-PAN with a $Zn(ClO_4)_2$

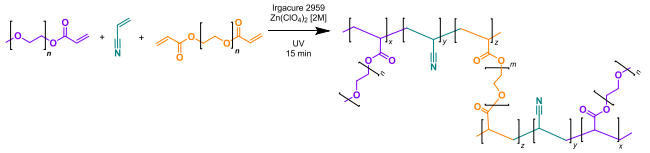

hydrogel electrolyte was synthesized from commercial materials by ultraviolet (UV) radical polymerization. At the beginning, 1.19 mL of PEGMEA (480 g mol^{-1}, 1.09 kg L^{-1}), 27 μL of AN (15 mol %, 53.06 g mol^{-1}, 0.8 kg L^{-1}), 17.5 μL of PEG-DA (2.5 mol %, 280 g mol^{-1}, 1.11 kg L^{-1}), and 2.47 mL of aqueous $Zn(ClO_4)_2$ solution (2 M) were mixed together. 7.2 mg of Irgacure 2959 (1 mol %) was dissolved in the monomer/electrolyte mixture. After homogenization, the mixture was placed in a UV cube and polymerized for 15 min. For other compositions, the mixture was always composed of 1.19 mL of PEGMEA (480 g mol^{-1}, 1.09 kg L^{-1}) and 27 μL of AN (15 mol %, 53.06 g mol^{-1}, 0.8 kg L^{-1}), and to this was added a calculated amount of PEG-DA (1, 2.5, or 4 mol %). The total volume was calculated, and $Zn(ClO_4)_2$ (2 M) was added in different proportions (1:2; 1:2.5). The amount of initiator (1 mol %) was recalculated for each monomer and added. After complete dissolution and homogenization, the mixtures were placed in a UV cube and polymerized for 15 min.

NMR Kinetic Studies. For kinetic studies *via* NMR, the same stock solution was prepared and divided into 12 samples, and the methyl groups of DMF (CH_3 2.89 ppm and CH 7.95 ppm) were used as an internal standard and the integral compared to that of the double bond signals of the monomers (5.9 to 6.0 ppm and 6.1 to 6.4 ppm) (Figure S1). ^1H spectra were recorded on a Bruker AC 300 spectrometer at 298 K. Chemical shifts are reported in parts per million (ppm, δ scale) relative to the residual signal of the deuterated solvent. Kinetic studies showed sufficient conversion of the monomers after 15 min of reaction time (Figure S2).

NMR $^1H/^{13}C$ HR-MAS. The samples were measured on an Avance III HD spectrometer with a 500 MHz magnet system and a 4 mm dual $^1H/^{13}C$ high-resolution-magic angle spinning (HR-MAS) sample head. The samples were swollen with D_2O (Figure S3). On the recorded spectra, the specific groups (nitrile, PEG, backbone for ^1H and nitrile, aliphatic, and carboxyl for ^{13}C) were identified and marked.

IR Spectroscopy. The IR method was used to measure the hydrogel electrolyte. For this purpose, the hydrogel electrolyte was measured for the first time immediately after polymerization. The same sample was then left to dry in the air for 2 weeks, and the measurement was then repeated. The same sample was frozen in nitrogen and lyophilized for 24 h. The sample was then measured immediately.

Synthesis of Poly(TEMPO-methacroloylamide) Active Material: One-Pot Electrode Preparation. The synthesis and oxidation toward PTMAm were adapted from the literature.[25] Oxidation degree *via* electron paramagnetic resonance (EPR) was 76.8 ± 5.4%

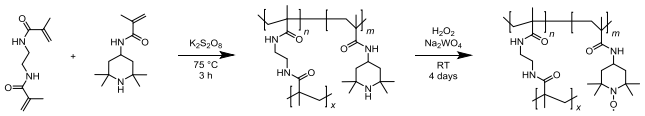

X-band EPR spectra were acquired on an EMXmicro CW-EPR spectrometer from Bruker, Germany. The SpinCountQ software module was used for determination of the spin count. A known PTMA polymer (radical content of 80%, determined through redox titration) was used as a reference. The radical contents of the TEMPO-containing compounds were determined from the mean values derived from the EPR spectra of three samples per compound.

Electrode and Battery Fabrication. Graphite discs (Ø 15 mm) were punched out of a graphite sheet and weighed individually. An electrode slurry was prepared from 60% PTMAm (250 mg), 35% SuperP (146 mg), and 5% PVDF (3.5 mL of 420 mg in 70 mL NMP solution). The mixture was left to swell overnight. The slurry was then stirred for 2 h at 4000 rpm with a dissolver (Dispermat, VMA-Getzmann GmbH, 25 mm blade). Subsequently, the slurry was placed onto the graphite discs via drop-casting and the discs were dried at 60 °C for 2 days. The electrodes were then weighed to calculate the material loading. Hydrogel electrolytes were prepared by mixing the described monomer solution and 2 M aqueous $Zn(ClO_4)_2$ solution and polymerizing the mixture in the UV

https://doi.org/10.1021/acs.jpcc.4c00654
J. Phys. Chem. C 2024, 128, 11465−11476

cube directly on the cathode, as described above. Coin cells (type 2032) were constructed from the prepared cathode/hydrogel composite and zinc foil discs (Ø 15 mm) as the anode.

Electrochemical Characterization Methods. All coin-cell electrochemical investigations were performed with a BioLogic BCS-805 battery cycler. Swagelok Cell experiments were performed using a BioLogic VMP-3 potentiostat. The obtained data were processed with BioLogic BT-Lab software (v1.69). Cells were left at RT for 12 h prior to battery testing. All testing protocols started with a 5 min OCV period. Potentio-controlled electrochemical impedance (PEIS) was measured with an amplitude of 10 mV in the region of 1 mHz to 1 Hz (60 data points per decade). Subsequently, 10 min of OCV was recorded before cyclic voltammetry (CV) was measured with 0.1, 0.2, 0.5, and 1.0 mVs^{-1} scan rates between 0 and 1.85 V for two cycles. Another 10 min of OCV recording was applied, followed by a 1C discharge to ensure that the material was discharged. Self-discharge tests were performed. The discharge capacities were then obtained after a charging period, followed by different subsequent OCV rest times. Rest times of 12, 24, 48, and 72 h were utilized. After self-discharge testing, the material was cycled at 1C for five cycles and at 5C until battery failure. With analog cells, after OCV, CV at 1 mVs^{-1}, and PEIS, rate capability tests were performed galvanostatically at 0.2C, 1C, 2C, 5C, 10C, 20C, and 50C for five cycles each. The rate capability tests were followed by float tests, which comprised 5 cycles of galvanostatic cycling at 1C, subsequently a 5 min of a 1C OCV period, then PEIS and finally the application of a voltage of 1.7 V for 10 h. This order was repeated until the battery failed.

The values for material usage were calculated without the oxidation degree factor, which of course revealed values lower than those in reality. The oxidation degree factor was intentionally avoided due to a relatively large error in the oxidation degree: The error varied from 2 to 9%. The presented values revealed the lowest material usage because they were drawn on an absolute theoretical maximum (100% oxidation degree).

X-ray Tomography. X-ray tomography was conducted using a cone-beam-based microcomputed tomography setup (μ-CT) manufactured in-house at Helmholtz Zentrum Berlin (HZB).[26] The μ-CT consisted of a Hamamatsu (L8121−3) X-ray source operated at 150 keV and a Hamamatsu flat panel detector (C7942SK-05) with a Gadox scintillator. The detector had a pixel size of 50 μm and was positioned at a 400 mm distance from the source. The sample was mounted onto a goniometer between the source and detector with a distance of 75 mm to the detector; thus, the setup yielded an image pixel size of 9.375 μm. The continuous X-ray spectrum was hardened using a 0.5 mm copper filter. 1200 projections (radiograms) were captured while rotating the sample over 360°. Each projection was exposed five times for 1.3 s each; additionally, 15 flat fields and 15 dark fields were captured. To avoid cone beam artifacts and to ensure an optimal reconstruction of the central parts of the coin cells, the cells were positioned flat with the positive electrode facing down in front of the center of the detector screen. After the measurements, the radiographic projections were normalized, denoised by means of total variation regularization, and reconstructed with the software Octopus 8.9.4 by XRE using a filtered back projection algorithm.[27,28] The final visualization was done using the software packages ImageJ/Fiji 1.53c (2D) and VG Studio Max 3.1 by Volume Graphics (3D).[29,30]

Stress−Strain Test. The hydrogels were prepared (polymerized) in a casting mold with dimensions according to ASTM standard method D38-14 type IV, with a total length of 115 mm and a width of 19 mm. Tensile tests were performed using a TIRAtest 2710 machine at a rate of 1 mm s^{-1} to failure.

Scanning Electron Microscopy (SEM). Scanning electron microscopy (SEM) imaging was performed with a Sigma VP field-emission scanning electron microscope (Carl-Zeiss AG, Germany) using an InLens and SE2 detector with an accelerating voltage of 6 kV.

Electrochemical Impedance Spectroscopy (EIS).[31] *EIS Measurements.* For all measurements, the following EIS settings were used in EC-Lab software. Mode: multisine, equilibration potential: 0.0000 V vs OCV, equilibration time t_E: 1 s, initial frequency: 1 MHz, final frequency: 100 Hz, number of points per decade: 10 (logarithmic), and voltage amplitude: 20 mV.

To measure the dependence of ionic conductivity on the temperature, the temperature was increased stepwise (from −20 to 50 °C; 10 °C each time) and kept constant for 3 h at each measured temperature. After 3 h, the EIS measurement was performed.

Film Thickness. After the EIS measurement, the total thickness of the hydrogel electrolytes was measured with a digital caliper gauge from the company Carl Roth.

Calculation of the Specific Conductivity. For each investigation, the specific hydrogel electrolyte conductivity was determined from the intercept of the Nyquist plot with the x-axis, the film thickness, and the area of the stainless-steel electrode (50 mm^2). Three samples were punched from each hydrogel electrolyte film, and each was measured three times. The values for the three samples (unless noted otherwise) were averaged to obtain representative specific hydrogel electrolyte conductivity.

RESULTS AND DISCUSSION

Investigation and Optimization of Hydrogel Electrolytes. For the synthesis of poly(ethylene glycol) diacrylate (PEG-DA)-cross-linked PEGMEA-*co*-PAN, photopolymerization was employed due to the simple handling, fast reaction times, and its compatibility with ambient conditions.

It is possible to prepare a PEGMEA-*co*-(PEG-DA)-*co*-PAN hydrogel electrolyte in two different ways. The first method is the bulk polymerization of the polymer matrix without electrolytes. After photoinitiated polymerization, the polymers are immersed in an electrolyte solution and allowed to swell. This approach is well established and widely used due to the simplicity of the method[32] but has shown poor reproducibility during swelling. This makes it difficult to use on a larger scale in industry. In addition, the swelling step is time-consuming.

The second method is a quasi-one-pot method. Contrary to the first method, the reaction occurs in solution. The monomer solution is mixed with the battery electrolyte prior to polymerization and polymerized directly. This method, which does not require any additional steps or reaction time, has shown high reproducibility in our previous work. Furthermore, direct polymerization on an electrode surface is possible with this preparation method for the hydrogel electrolytes. This can be applied to button cell batteries, where preprepared electrode discs can be directly covered with the conductive

https://doi.org/10.1021/acs.jpcc.4c00654
J. Phys. Chem. C 2024, 128, 11465−11476

Table 1. Different Monomer and Monomer/Electrolyte Compositions with Resulting Ionic Coductivity [mS cm^{-1}] and Flexibility [%]

monomer composition main monomer/cross-linker/acryl nitrile	monomers/electrolyte [vol/vol]	ionic conductivity [mS cm^{-1}]	flexibility [%]
PEGMEA/TMPETA(1 mol %)/AN(15 mol %)	1:2	12.1 ± 1.9	50
PEGMEA/TMPETA(1 mol %)/AN (15 mol %)	1:2.5	15.8 ± 2.4	75
PEGMEA/PEG-DA(2.5 mol %)/AN(15 mol %)	1:2	18.4 ± 1.0	400
PEGMEA/PEG-DA(2.5 mol %)/AN(15 mol %)	1:2.5	–[a]	–[a]
PEGMEA/PEG-DA(4 mol %)/AN(15 mol %)	1:2.5	17.1 ± 0.6	550

[a]Pressure-unstable films, no measurement could be performed.

and separating hydrogel. Compared with the preparation of a free-standing hydrogel, this process achieves better contact between the electrode and the electrolyte, which improves the accessibility of the active material molecules in the electrode.

In addition, this approach eliminates the manufacturing steps of punching out the gel and transferring it to the button cell. Both of these steps can cause (micro) cracks in the hydrogel and on its surface, resulting in reduced conductivity of the electrolyte and reduced contact between the hydrogel and the composite electrode, respectively.

The hydrogel was prepared from monomers selected for their high hydrophilicity, water solubility, and commercial availability. The monomers have previously been used for their interesting mechanical properties, both in homopolymers and in different functional copolymer systems.[33−35] Recently, the system of PTMAm and zinc was described by Schröter et al. to be compatible with different water-soluble zinc salts.[25] The investigated salts included $Zn(OTf)_2$, $ZnTFSI_2$, and $Zn(ClO_4)_2$. The described systems have shown high rate capabilities and good stabilities (capacity retention of 99% after 1000 cycles at 5C). On the basis of these previous results, $Zn(ClO_4)_2$ was chosen as the electrolyte salt for the present hydrogels. Additionally, this salt revealed the highest ionic conductivity in comparison to other zinc salts like $Zn(OTf)_2$ or $ZnTFSI_2$ and was significantly more cost-efficient.

Hydrogel mechanical properties depend on several parameters, the most important being the type of cross-linker selected and its proportion in the monomer mixture. In general, the cross-linkers differ in the number of reactive groups that they contain. In this work, we have studied cross-linkers with two and three reactive groups, namely, diacrylates and triacrylates. We used different concentrations and their influence on the mechanical properties and ionic conductivities of the hydrogel electrolytes. A high proportion of cross-linker leads to a polymer matrix that is rigid, brittle, and unstable under pressure. In addition, a high degree of cross-linking resulted in a close-meshed network, which can reduce the mobility of the ions in the electrolyte. On the other hand, a low concentration should also be avoided as this will result in a lower number of cross-linking points, leading to a higher proportion of linear polymer chains. In addition, some monomers may remain unpolymerized or oligomerized. Low molar mass linear components could then diffuse out of the polymer matrix and negatively affect battery performance. Besides poly(ethylene glycol) diacrylate (PEG-DA), trimethylolpropane ethoxylate triacrylate (TMPETA) was also initially used as a cross-linker. However, the TMPETA cross-linker led to a low elasticity of the films and was therefore abandoned (Table 1).

PEG-DA, on the other hand, gave suitable films with higher flexibility. Furthermore, acrylnitrile (AN) was introduced as a comonomer in the polymer matrix, as it is widely used in various industrially known polymers due to its positive influence on mechanical properties, such as compression set, elasticity, and low-temperature flexibility. First, the ideal PEG-DA/PAN/$PEGMEA_{aq}$ $Zn(ClO_4)_2$ ratio was elucidated. For this purpose, impedance measurements were made on each hydrogel electrolyte, and the ionic conductivity was calculated. In addition, each film was manually tested for flexibility and bendability. Sufficient mechanical properties and high ionic conductivity were the key parameters to continue using the hydrogel electrolyte. The preparation and synthesis of the hydrogel electrolytes were carried out in a few steps, which are shown in Figure 1. First, all components, such as monomers,

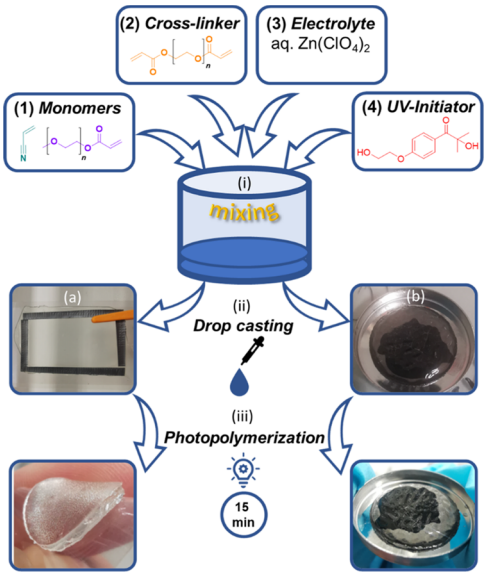

Figure 1. Preparation of the hydrogel electrolyte. (i) Mixing of monomers, UV initiator, and aqueous electrolyte solution, (ii) (a) drop-casting onto the Mylar film in a frame to produce a free-standing hydrogel, (b) drop-casting directly onto the cathode surface, and (iii) UV polymerization in a UV cube during 15 min.

electrolyte, and initiator, were combined and homogenized. After complete dissolution of the initiator, the mixture was cast onto a Mylar foil to obtain a free-standing hydrogel or directly onto the polymer composite electrode, followed immediately by the photopolymerization in a UV cube for 15 min. The reaction kinetics (see the Supporting Information) of the photopolymerization was studied by NMR spectroscopy and revealed that the conversion did not reach 100% after 15 min as well as after 20 min. The determination of the conversion showed that about 6% of the monomers remained unconsumed after each polymerization. The photopolymerization cannot be carried out for longer than 20 min due to the increasing temperature in the UV cube, which can lead to the

https://doi.org/10.1021/acs.jpcc.4c00654
J. Phys. Chem. C 2024, 128, 11465−11476

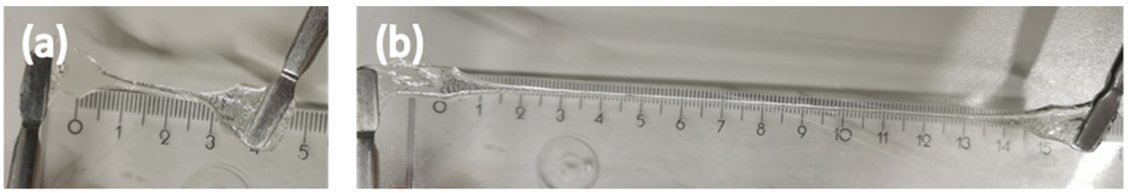

Figure 2. Optical images of PEGMEA-*co*-PEG-DA-*co*-AN while stretching to 400% (a, b).

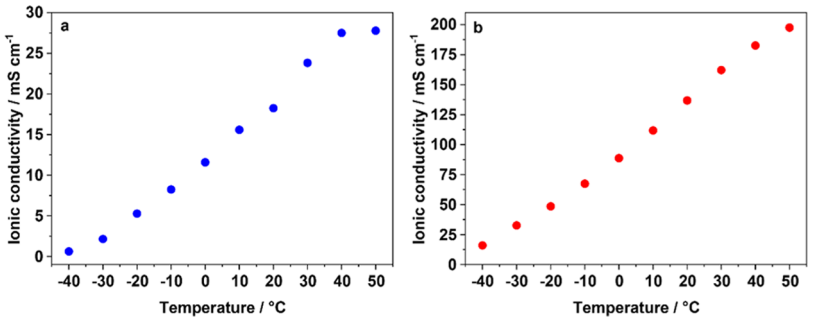

Figure 3. Temperatur dependence of the ionic conductivity of the hydrogel electroylte (a) and conventional aqueous 2 M $Zn(ClO_4)_2$ electrolyte (b) between −40 and 50 °C in 10 K steps.

evaporation of water. Next, the optimal electrolyte-to-monomer ratio was determined. For this purpose, the electrolyte amount that was used to dissolve the monomers prior to polymerization was varied. Three compositions were thoroughly studied, namely, monomer-solution/electrolyte-solution volume ratios of 1:2 and 1:2.5 (Table 1). Hydrogels with low water content showed medium ionic conductivity and were not elastic and pressure stable, while hydrogels with high electrolyte content were very sticky, which severely hampered further use. The hydrogel resulting from the 1:2 ratio showed the most suitable flexibility and high ionic conductivity (20 ± 1 mS cm^{-1}). The maximum strain was determined by a tensile strain test and was around 400% (Figure 2). Additionally, the hydrogel electrolytes were analyzed by IR and HR-MAS NMR spectroscopic studies (see the Supporting Information).

For Young's modulus, identically prepared hydrogels (1:2 ratio) were investigated and measured identically. By these means, the reproducibility of the performed synthesis should be investigated. The calculated Young's modulus revealed only a small deviation (0.018 kPa ± 9%), which means that the polymerized hydrogels are rather identical to each other, which provides a hint toward a high reproducibility of the polymer synthesis.

To investigate the feasibility of the hydrogels for batteries at different operating temperatures, the ionic conductivity was measured over a temperature range of −40 to 50 °C. (Figure 3 and Table 2). The hydrogel electrolyte behavior resembles the typical behavior of aqueous electrolytes.[36] It was expected that low temperatures would lead to lower ionic mobility and water crystallization, which, in turn, would negatively affect ionic mobility. Therefore, the conductivity at low temperatures is expected to be very low, reaching 0.6 mS cm^{-1} at −40 °C. Although these values are low, the hydrogel electrolyte still has a certain amount of conductivity. This is due to the fact that the salt ions of the supporting electrolyte can alter the freezing point of water so that complete freezing does not occur below 0 °C. In addition, the chains of the polymer matrix may also play a small role in this and may support this effect.[37] The incorporated AN units are known to mediate a certain flexibility to the chains at low temperatures.[38,39] In general, this is expected to make the polymer matrix rather flexible, which could support ion transport through the medium. Above approximately 40 °C, the ionic conductivity differs only very slightly (0.3 mS cm^{-1}) between the measured temperatures, which may indicate that the maximum achievable conductivity is close to this value (27.8 mS cm^{-1}). Greater values are probably not obtainable due to the polymer matrix limiting the diffusion of the free ions in the hydrogel electrolyte and the fact that the conductivity is intrinsically limited by the total number of ions in the electrolyte.

Table 2. Ionic Conductivity with Varying Temperatures

temperature [°C]	ionic conductivity [mS cm^{-1}]
−40	0.6 ± 0.4
−30	2.1 ± 1.0
−20	5.3 ± 0.4
−10	8.2 ± 0.5
0	11.6 ± 0.4
10	15.6 ± 0.5
20	18.3 ± 1.9
30	23.8 ± 0.5
40	27.5 ± 0.7
50	27.8 ± 1.0

Electrochemical Characterization. To investigate if the present hydrogel can work as an alternative for a conventional separator/electrolyte combination, a literature-known battery system was taken as a reference, and the separator was exchanged for the new hydrogel. Namely, the previously described PTMAm−zinc system was adapted and the measurements were performed accordingly.[25] Apart from the utilized electrolyte modification, the systems were constructed identically with a 2 M $Zn(ClO_4)_2$ supporting electrolyte.

Figure 4 shows the cyclic voltammograms of PTMAm in the semiorganic coin cells. Both systems revealed reversible oxidation and reduction peaks with similar same half-wave potentials (hydrogel cell: 1.48 V and reference aqueous cell: 1.49 V).

https://doi.org/10.1021/acs.jpcc.4c00654
J. Phys. Chem. C 2024, 128, 11465−11476

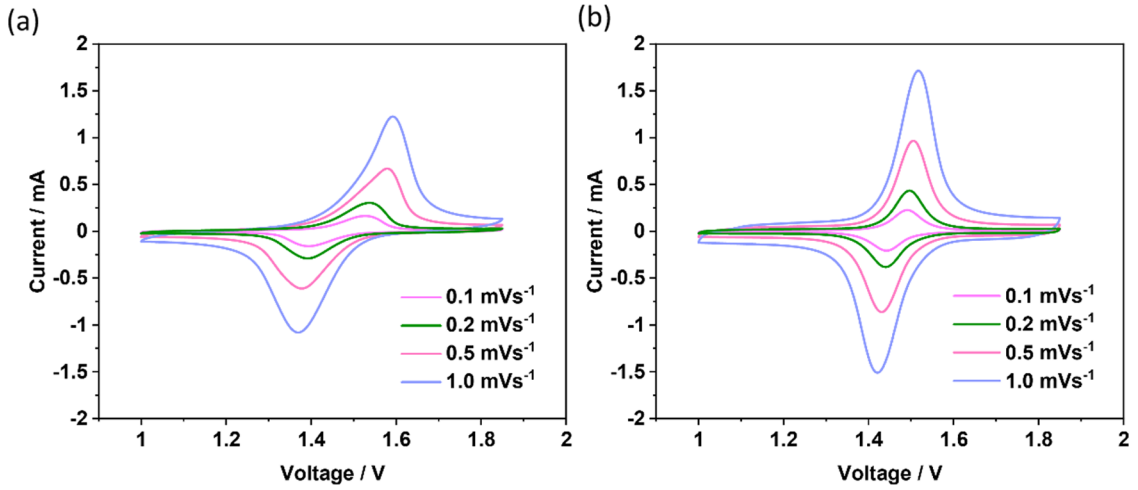

Figure 4. Cyclic voltammetry measurements of PTMAm/Zn coin cells at 0.1, 0.2, 0.5, and 1.0 mVs^{-1} scanning rates and different electrolytes. (a) Hydrogel electrolyte and (b) liquid electrolyte containing $Zn(ClO_4)_2$ with a glass fiber separator.

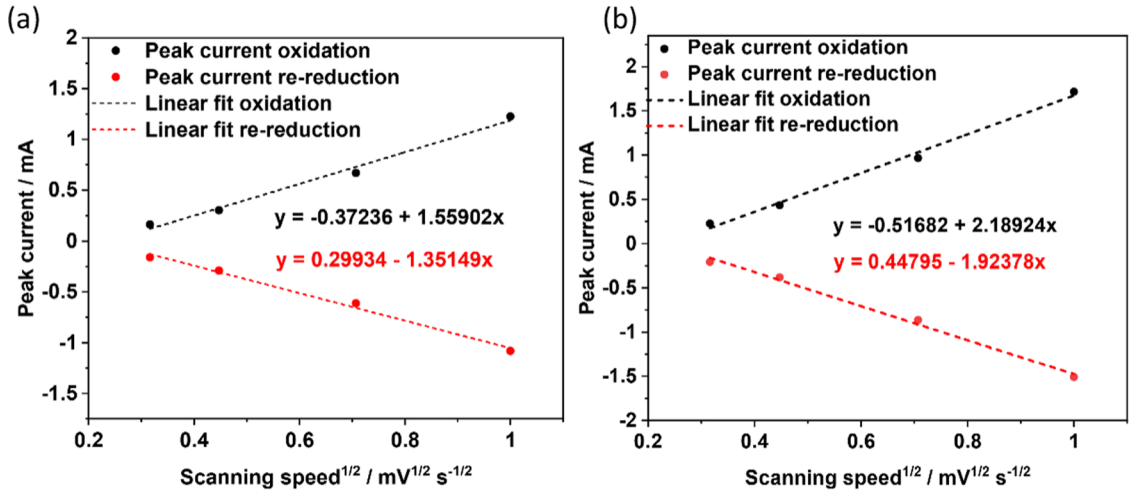

Figure 5. Plot of the peak currents vs the square root of the scanning speeds from the cyclic voltammetry analysis of the batteries during the CV testing. (a) Hydrogel electrolyte and (b) liquid electrolyte containing $Zn(ClO_4)_2$ with a glass fiber separator. Linear fit.

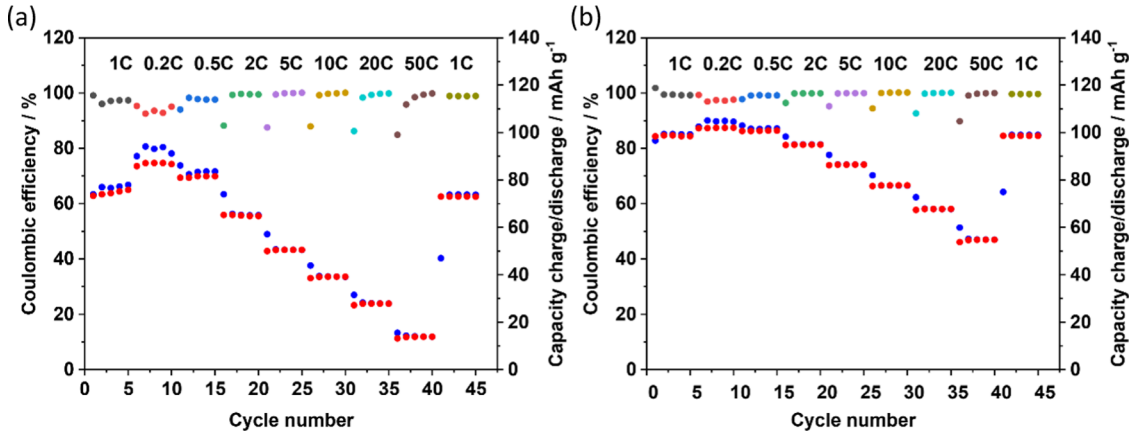

Figure 6. Charging rate tests for PTMAm/Zn batteries (a) with hydrogel electrolyte and (b) with 2 M $Zn(ClO_4)_2$ aqueous solution as supporting electrolytes.

For both systems, the peak currents correlate linearly with the square roots of the applied scan rates, which is evidence of diffusion-controlled kinetics (Figure 5). However, it should be noted that the oxidation signals for the hydrogel cells exhibited a broadening and a larger peak split at all investigated scan rates compared to the reference cells. This is referred to the reduced diffusion inside the hydrogel, as both the diffusion of ions to the electrode surface and the subsequent transition

https://doi.org/10.1021/acs.jpcc.4c00654
J. Phys. Chem. C 2024, 128, 11465−11476

from the hydrogel to the active material are slower compared to a liquid electrolyte, where ions can migrate rather freely. While the diffusion limitation, related to the hydrogel electrolyte, might result in higher cell resistances, the CV analysis proved that the active moieties of the composite cathode are still addressed even though no liquid electrolyte is utilized.

After the CV experiments, the cells were subjected to galvanostatic battery cycling at different charging/discharging rates. Charging rates from 0.2 and 50C were tested, and the corresponding capacities can be obtained from Figure 6. The experiments based on the hydrogel electrolyte revealed that, at high rates, lower capacities were achieved and worse material utilization was obtained. This behavior is pronouncedly observed for the hydrogel cells, as the charging rate is expected to play a higher role compared to the reference cell due to the slower diffusion processes in the gel. The higher charging currents did not cause degradation of the PTMAm active material, as can be seen in the last five cycles at 1C, where comparable capacities were obtained as for the initial 1C charging rates. However, the two systems differ in the achieved capacities and calculated material usage, which are shown in Table 3. The aqueous electrolyte systems revealed higher

Table 3. Material Usage [%] at Different Charging Rates (1C, 0.2C, 0.5C, 2C, 5C, 10C, 20C, 50C) with the Hydrogel System and the Conventional Liquid Electrolyte

	material usage of active material in batteries with	
charging rate	hydrogel system [%]	liquid electrolyte [%]
1C	67.4	88.5
0.2C	78.4	91.4
0.5C	73.3	90.4
2C	58.5	85.1
5C	45.5	77.5
10C	35.3	69.7
20C	25.0	60.7
50C	12.4	49.1
1C	65.7	88.4

material utilization and specific capacities at all C-rates, which can be explained by the significantly higher material wetting with the solution compared to the polymer matrix.

To investigate the shelf life of the presented battery system, the cells were subjected to self-discharge experiments. For this purpose, an established method by Gerlach and Balducci was utilized.[40] During these experiments, the cells were charged and left at open-circuit conditions for 12, 24, 48, and 72 h. The self-discharge was determined through the ratio of the charge capacity and discharge capacity before and after the OCV period, respectively. The calculated capacity retention after self-discharge is shown in Figure 7.

In both systems, capacity loss could be observed. The first large-capacity decrease appears to happen in the initial 12 h for both the conventional and the hydrogel cell. However, the compared cells behave differently from this point onward. While the conventional battery retained most of its capacity even at longer OCV times, the hydrogel battery loses a significant part of its capacity uniformly over the course of 72 h. The faster self-discharge process in hydrogel cells can be explained by the presence of remaining monomers or oligomers that have not reacted during the free radical polymerization and can diffuse into the cathode surface

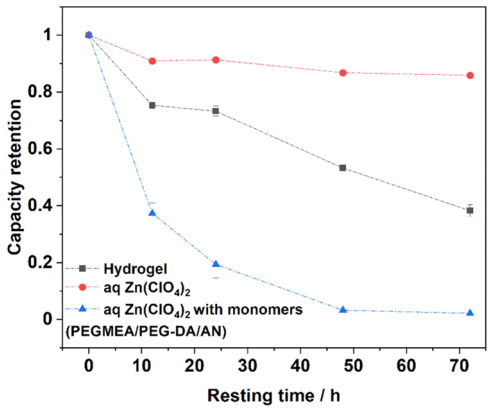

Figure 7. Percentage of retained capacity after self-discharge for the PTMAm/Zn batteries with (black) hydrogel electrolyte and (red) aq. $Zn(ClO_4)_2$ and (blue) aq. $Zn(ClO_4)_2$ with monomers (PERMEA/AN/PEG-DA) at different resting times.

under these conditions, where they can cause undesired side reactions. This assumption is supported by an analog test of batteries with an electrolyte that consisted of aq $Zn(ClO_4)_2$ as well as the used monomers (PEG-DA, AN, PEGMEA). The experiment revealed that the addressable capacity was almost completely lost after 48 h (about 3%). This indicates that the unreacted monomers destroy the active material of the cathode.

Float tests were performed to examine the resilience of the materials under harsh potentiostatic charging conditions. The float test was conducted for 500 h for both battery systems (Figure 8). During the experiment, a constant charging voltage

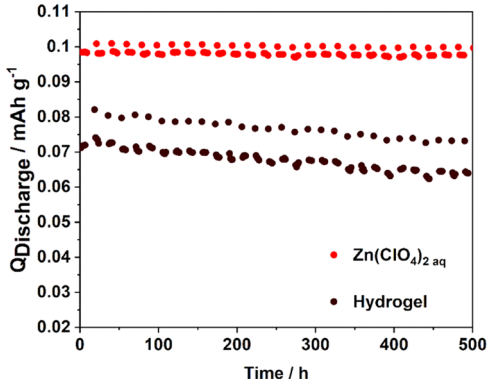

Figure 8. Charging capacities during float tests for the PTMAm/Zn cells with a hydrogel (black) and liquid electrolyte (red). Voltage of 1.7 V was held for 10 h, and then five cycles at 1C were performed.

of 1.7 V was applied for 10 h, after which the batteries were cycled galvanostatically at 1C for five cycles. This approach is expected to reveal possible weaknesses during long-term charging and instabilities in the charged state. The reference cells showed very stable behavior over time. At the beginning, the cells revealed 98.5 mAh g^{-1} discharge capacity; after 500 h, the value changed marginally to 97.6 mAh g^{-1}, which corresponds to 99% capacity retention. In contrast, the initial discharge capacity of the hydrogel cells was 74.1 mAh g^{-1} and dropped slowly to 64.3 mAh g^{-1} after 500 h. This corresponds to a lower capacity retention of 87% and suggests that the hydrogels may have an impact on the battery performance under the strong constant voltage stress. At this point, the

https://doi.org/10.1021/acs.jpcc.4c00654
J. Phys. Chem. C 2024, 128, 11465−11476

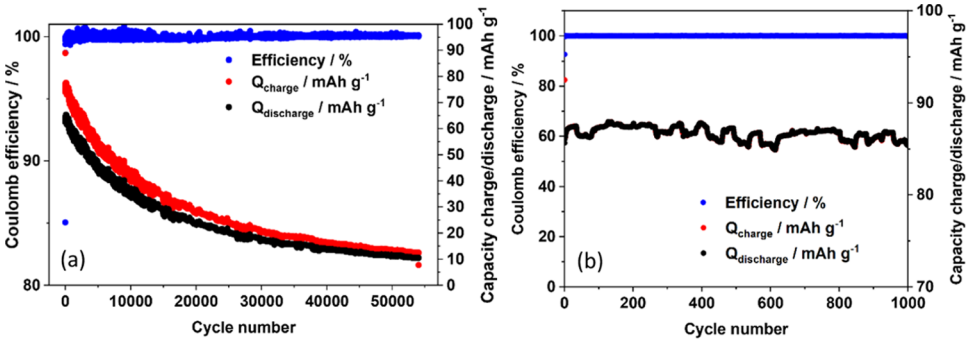

Figure 9. Efficiencies of charge and discharge capacities for the long-term cycling of the PTMAm/Zn cells at 5C utilizing (a) hydrogel and (b) liquid electrolyte.

same explanation applies as that for the self-discharge test: The unreacted monomers can cause parasitic reactions on the cathode side, leading to a slow discharge of the electrode. In addition, the monomers are able to partially dissolve PVdF, which was observed during the optimization of the double-drop-casting method. This led to the release of the cathode components into the electrolyte, which can provoke shuttle processes and promote discharging

Finally, the long-term stability of the coin cells was examined. For this purpose, the batteries were cycled at 5C until no significant capacity remained to demonstrate the stability of the electrode materials during cycling. The achieved efficiencies and charge−discharge capacities are shown in Figure 9. For the conventional electrolyte, 1000 cycles could be measured until the test cells started to fail. This is associated with dendrite growth in the cells, which is often observed in zinc-based batteries.[25] However, for 1000 cycles, the material exhibited stable cycling with a very high capacity retention of 99.7% after 1000 cycles and constant Coulombic efficiencies of >99%.

In comparison, the measured hydrogel batteries exhibited extremely high long-term stability. All tested batteries could be operated for over 50,000 cycles. The slowly descending capacity curve revealed a slight degradation of the batteries (Table 4). The capacity retention after 1000 cycles was a bit lower compared to the batteries with the aqueous electrolyte (91%). This difference can be explained by the fact that the Whatman separator in the reference batteries was completely inert and had no influence on the degradation of the active material on the cathode side. The hydrogel, on the contrary, as it was described earlier, may have a small amount of reactive monomers or even short non-cross-linked polymer chains that can migrate to the electrodes over time. Compared with the inert Whatman separator, the remnants may cause a deleterious effect. Despite a slightly lower capacity retention after the initial 1000 cycles, an excellent overall cycling stability was observed. After 7500 cycles, over 60% of the initial capacity was retained. The largest capacity loss per cycle occurred around the 1000th cycle. Afterward, the loss per cycle slowly decreased. This can be explained by the fact that the number of redox active moieties decreases over time, in particular, those redox active units directly at the interface between the cathode and the hydrogel. The remaining units are located in deeper layers and are thus better protected from the possible migrating byproducts of the hydrogel and from the general aging process. Another possible explanation is that the number of unreacted monomers decreases over time due to side reactions. When the monomers disappear completely, the degradation process of the active material slows or stops completely.

Table 4. Cycle Number and Corresponding Calculated Capacity Retention [%] and Loss Per Cycle [%] for Galvanostatic Long-Term Cycling at 5C

cycle number	capacity retention [%]	loss per cycle [%]
250	99.7	0.0012
500	98.5	0.0030
750	96.0	0.0053
1000	91.0	0.0093
2500	80.6	0.0086
5000	71.7	0.0066
7500	60.3	0.0067
15,000	42.9	0.0056
30,000	27.5	0.0043
40,000	21.3	0.0039
50,000	17.8	0.0034

Nevertheless, the hydrogel batteries revealed no sudden capacity decay and no short circuits. This indicates that the hydrogel fulfills an additional function, namely, the inhibition of dendrite growth. In liquid aqueous electrolytes, dendrite growth cannot be avoided without supplementary additives or special treatment of the zinc surface.[41] This is due to the fact that the crude zinc electrode can show impurities or an uneven surface if non-pretreated. Protruding peaks on the zinc surface can interact with the zinc ions due to a shortened diffusion path, and in addition, the peaks can generate a strong electric field, so that more Zn^{2+} accumulates and deposits near these peaks. By this way, dendrites are formed, which can penetrate the separator to create a short circuit.

SEM and Tomography Measurements. Compared to liquid electrolytes, hydrogels do not only show high ionic conductivity but also other advantages, such as a fairly high mechanical stability of the hydrogel, which provides protection against dendrites, when metal electrodes, e.g., zinc, are used. Hydrogels consist of a 3D polymer matrix, which enables a 3D diffusion process, as the channel structure restricts the random movement of ions.[42] Furthermore, poly(ethylene oxide)- and acryl nitrile-based polymer electrolytes feature a large number of functional groups providing free electron pairs of heteroatoms, such as oxygen or nitrogen, which can possibly interact with ions.[43]

Lou et al. described an influence of nitrogen atoms on cobalt ions, namely, a coordination of cobalt ions via the free electron pairs of the nitrogen atoms.[44] Lin et al. have found with the

https://doi.org/10.1021/acs.jpcc.4c00654
J. Phys. Chem. C 2024, 128, 11465−11476

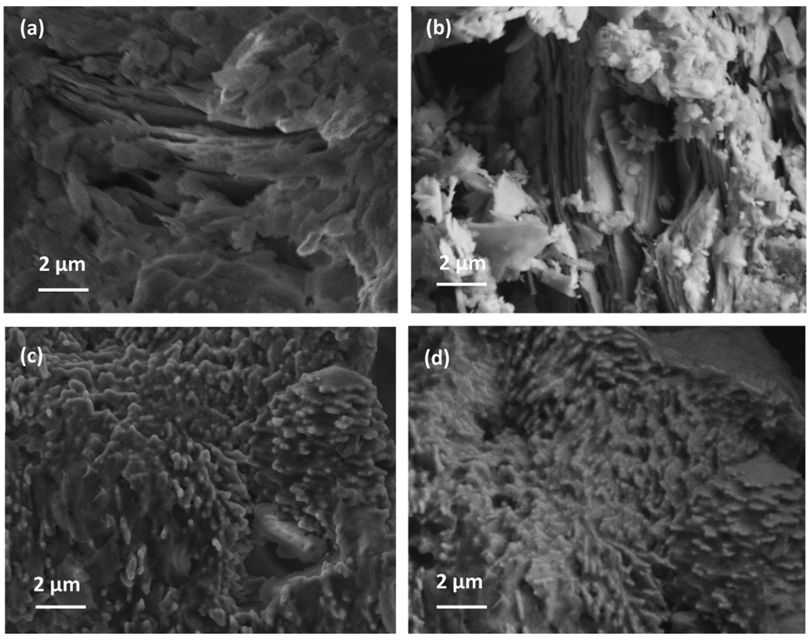

Figure 10. Influence of electrolytes on the zinc anode surface. SEM image of the zinc anode of a PTMAm/Zn battery after cycling for ca. 2000 cycles using a liquid electrolyte (a, b) and a hydrogel (c, d).

help of density functional theory (DFT) calculations that the amino groups can serve as formation sites for the storage of lithium atoms.[45] Also, Yang et al. investigated the lithium dendrite suppression via the combination of DFT calculations and Raman spectroscopy.[46] It was found that the lithium ions and the used electrolytes (tetraethylene glycol dimethyl ether/1,2-dimethoxyethane/1,3-dioxolane) show a strong coordination interaction with each other. The strong coordination leads to a slower electrochemical reaction rate, and as a result, the lithium electrodeposition rate decreases suppressing the dendrite formation. A similar process is imaginable for zinc ions. The dendrite formation was studied in more detail in Swagelok-type cells. Hydrogel and liquid electrolyte cells were cycled at 5C until the dendrite-caused short circuit was observed. The electrode discs were then removed from the cells and subjected to electron microscopy to confirm the formation of dendrites in the cell (Figure 10).

The SEM images of the zinc on the reference battery revealed many nonordered zinc sheets randomly stacked on top of each other, comparable to images presented in the respective literature.[41,,48] In contrast, the images of zinc from the hydrogel batteries looked completely different. It can be seen that the zinc electrode surface is rough, and it does not show zinc sheets but flat rounded species. The images are comparable to the images presented in the work by Hao et al.[49]

The dendrite growth was further investigated via X-ray tomography. Figure 11 shows a 3D rendering image of the different inner layers of the cell, with the blue arrow indicating the studied zinc electrode.

The 3D reconstruction of X-ray tomography made it possible to generate sectional images of the operated button cells. The images in Figure 12 represent straight virtual cuts through the center of the cells and 3D representations of the zinc electrodes: (a) Investigation of a freshly built, noncycled reference cell with the aqueous $Zn(ClO_4)_2$ electrolyte. The measurement revealed no irregularities on the surface. Images (b) and (c) present a cycled reference cell with the aqueous electrolyte: The dendrites, which were highlighted in yellow in

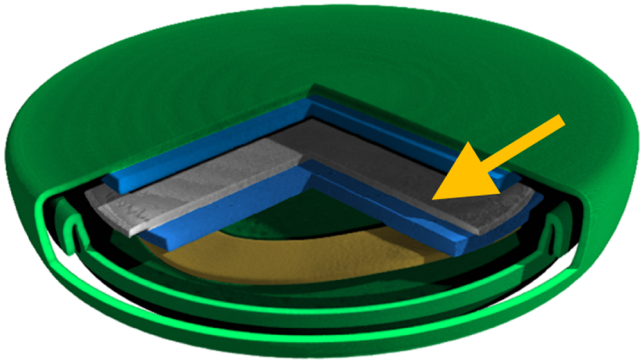

Figure 11. 3D render image of the inside of the cell; the yellow arrow marks the zinc (rendered in gray shades) electrode.

the 3D representation, are sporadically distributed all over the surface; several are observed at the edge of the electrode. The last graphs (d) and (e) show the hydrogel electrolyte cell that exhibited no dendrite formation. However, some irregularities such as holes on the surface can be seen that might result from scratches in the zinc surface that were present prior to the cell assembly.

It can be concluded that dendrite formation is significantly hindered in the hydrogel-containing cells. Most probably, the mechanical resistance in combination with the electrochemical interactions between the hydrogel and the supporting electrolyte, which was described before, is the reason for this behavior. By this means, one of the main disadvantages of the semiorganic zinc-polymer battery is overcome, expanding the application potential of this system.

CONCLUSIONS

In conclusion, we successfully designed a hydrogel electrolyte for organic batteries with excellent cycle stability and high capacity retention. The cross-linked hydrogel electrolyte was synthesized by photoinitiated polymerization of commercially available monomers in an electrolyte solution. The hydrogel

https://doi.org/10.1021/acs.jpcc.4c00654
J. Phys. Chem. C 2024, 128, 11465−11476

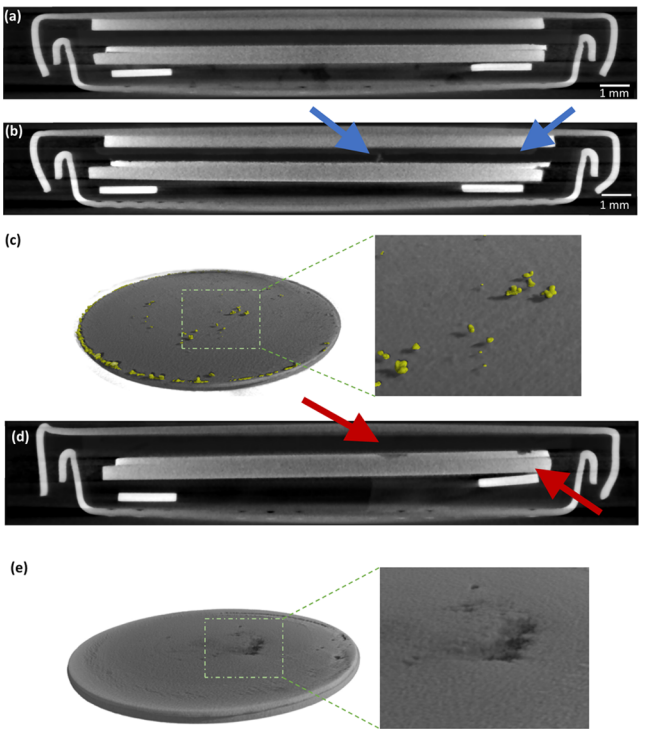

Figure 12. X-ray tomography images of the Zn/PTMAm coin cells. (a) With liquid aq. $Zn(ClO_4)_2$ electrolyte before cycling and (b) after 2750 cycles (blue arrows indicate dendrite growth); (c) zinc anode after 2750 cycles; (d) With the hydrogel separator after 20,000 cycles (red arrows indicate hole-like irregularities); (e) zinc anode after 20,000 cycles.

electrolyte features high ionic conductivities at room temperature (20 ± 1 mS cm^{-1}) and still good ionic conductivity at low temperatures (5.3 ± 0.3 mS cm^{-1} at -20 °C), which can be attractive for further application scenarios, for example, for smart textiles or packaging. Furthermore, we developed and optimized a direct casting and polymerization procedure on the cathode surface. The method provides improved contact at the electrolyte/electrode interface at a molecular level and presents better wetting and lower resistance between the electrode and hydrogel interfaces. The method also simplifies the battery assembly. Direct polymerization avoids any mechanical deformation of the hydrogel.

Microscopic and tomographic studies also showed that the formation of dendrites during cycling can be effectively inhibited when the electrolyte is used with a zinc electrode. In comparison to a liquid electrolyte reference system, the hydrogel cells did not fail due to dendrite-mediated short-circuiting but retained the electrochemical performance of the reference cells, making the polymer electrolyte also suitable for batteries with metal electrodes, in particular zinc-based systems. In conclusion, with the demonstrated hydrogel, we present a highly attractive, upscalable, and straightforward approach toward sustainable, aqueous, and nonleakable organic battery electrolytes.

For future work, it is, of course, possible to improve certain parameters. An application of suitable additives, e.g., SiO_2, can change the viscosity of the monomer/electrolyte mixture and, thus, one could make the application of the mixture to the cathode before the polymerization easier. Regarding the battery performance, the usage of other monomers can positively influence the mobility of the ions and increase the ionic conductivity. Finally, the main focus is the development and production of a fully organic battery with a hydrogel electrolyte.

■ ASSOCIATED CONTENT

Supporting Information

The Supporting Information is available free of charge at https://pubs.acs.org/doi/10.1021/acs.jpcc.4c00654.

Exemplary series of ^{1}H NMR kinetic study on hydrogel electrolyte PEGMEA/PEG-DA(2.5 mol %)/AN(15 mol %) with monomers/electrolyte [1:2 vol/vol] (300 MHz, DMSO-d_6, δ in ppm) (Figure S1); conversion of the monomers during the photoinitiated polymerizaton as obtained from the NMR kinetic studies (Figure S2); ^{1}H spectrum of hydrogel electrolyte after dialysis and freeze drying (500 MHz, D_2O, δ inppm) (Figure S3); ^{13}C spectrum of hydrogel electrolyte after dialysis and freeze drying (500 MHz, D_2O, δ in ppm) (Figure S4); IR spectra of hydrogel-electrolyte: directly after polymerization, 2 weeks after polymerization, freeze-dried polymer (Figure S5); optical images of the PEGMEA-*co*-PEG-DA-*co*-AN while stretching with tensile machine and stress-strain curves of the hydrogel electrolytes (Figure S6) (PDF)

■ AUTHOR INFORMATION

Corresponding Author

Ulrich S. Schubert − *Laboratory of Organic and Macromolecular Chemistry (IOMC), Friedrich Schiller University Jena, 07743 Jena, Germany; Center for Energy and Environmental Chemistry Jena (CEEC Jena), Friedrich Schiller University Jena, 07743 Jena, Germany; Helmholtz Institute for Polymers in Energy Application Jena (HiPOLE Jena), 07743 Jena, Germany;* orcid.org/0000-0003-4978-4670; Email: ulrich.schubert@uni-jena.de

Authors

Lada Elbinger − *Laboratory of Organic and Macromolecular Chemistry (IOMC), Friedrich Schiller University Jena, 07743 Jena, Germany; Center for Energy and Environmental Chemistry Jena (CEEC Jena), Friedrich Schiller University Jena, 07743 Jena, Germany*

Erik Schröter − *Laboratory of Organic and Macromolecular Chemistry (IOMC), Friedrich Schiller University Jena, 07743 Jena, Germany; Center for Energy and Environmental Chemistry Jena (CEEC Jena), Friedrich Schiller University Jena, 07743 Jena, Germany;* orcid.org/0000-0001-8388-1437

Philip Zimmer − *Laboratory of Organic and Macromolecular Chemistry (IOMC), Friedrich Schiller University Jena, 07743 Jena, Germany; Center for Energy and Environmental Chemistry Jena (CEEC Jena), Friedrich Schiller University Jena, 07743 Jena, Germany*

Christian Friebe − *Laboratory of Organic and Macromolecular Chemistry (IOMC), Friedrich Schiller University Jena, 07743 Jena, Germany; Helmholtz Institute for Polymers in Energy Application Jena (HiPOLE Jena), 07743 Jena, Germany;* orcid.org/0000-0001-8587-6658

Markus Osenberg − *Institute of Applied Materials, Helmholtz-Zentrum Berlin für Materialien und Energie (HZB), 14109 Berlin, Germany*

Ingo Manke − *Institute of Applied Materials, Helmholtz-Zentrum Berlin für Materialien und Energie (HZB), 14109 Berlin, Germany; Helmholtz Institute for Polymers in Energy Application Jena (HiPOLE Jena), 07743 Jena, Germany;* orcid.org/0000-0001-9795-5345

Complete contact information is available at: https://pubs.acs.org/10.1021/acs.jpcc.4c00654

Notes

The authors declare no competing financial interest.

■ ACKNOWLEDGMENTS

We gratefully acknowledge the financial support of the Thüringer Aufbaubank (TAB, project 2019 FGR 0080) and the German Research Council (DFG, SPP 2248 441292784). We thank Steffi Stumpf for the measurements of the SEM images. The SEM facilities of the Jena Center for Soft Matter (JCSM) were established with a grant from the DFG. We thank Dr. Izabela Firkowska-Boden for the measurements of the tensile tests.

■ REFERENCES

(1) Dunn, B.; Kamath, H.; Tarascon, J.-M. Electrical Energy Storage for the Grid: A Battery of Choices. *Science* **2011**, *334*, 928−935.
(2) Larcher, D.; Tarascon, J. M. Towards greener and more sustainable batteries for electrical energy storage. *Nat. Chem.* **2015**, *7*, 19−29.
(3) Nitta, N.; Wu, F.; Lee, J. T.; Yushin, G. Li-ion battery materials: present and future. *Mater. Today* **2015**, *18*, 252−264.
(4) Hannan, M. A.; Lipu, M. S. H.; Hussain, A.; Mohamed, A. A review of lithium-ion battery state of charge estimation and management system in electric vehicle applications: Challenges and recommendations. *Renewable Sustainable Energy Rev.* **2017**, *78*, 834−854.
(5) Zhong, C.; Deng, Y.; Hu, W.; Qiao, J.; Zhang, L.; Zhang, J. A review of electrolyte materials and compositions for electrochemical supercapacitors. *Chem. Soc. Rev.* **2015**, *44*, 7484−7539.
(6) Wang, Z.; Li, H.; Tang, Z.; Liu, Z.; Ruan, Z.; Ma, L.; Yang, Q.; Wang, D.; Zhi, C. Hydrogel electrolytes for flexible aqueous energy storage devices. *Adv. Funct. Mater.* **2018**, *28*, No. 1804560.
(7) Arora, P.; Zhang, Z. Battery Separators. *Chem. Rev.* **2004**, *104*, 4419−4462.
(8) Ye, Z.; Cao, Z.; Chee, M. O. L.; Dong, P.; Ajayan, P. M.; Shen, J.; Ye, M. Advances in Zn-ion batteries via regulating liquid electrolyte. *Energy Storage Mater.* **2020**, *32*, 290−305, DOI: 10.1016/j.ensm.2020.07.011.
(9) Guo, Z.; Wang, T.; Wei, H.; Long, Y.; Yang, C.; Wang, D.; Lang, J.; Huang, K.; Hussain, N.; Song, C.; et al. Ice as Solid Electrolyte To Conduct Various Kinds of Ions. *Angew. Chem. Int. Ed* **2019**, *58*, 12569−12573.
(10) Li, X.; Li, M.; Yang, Q.; Li, H.; Xu, H.; Chai, Z.; Chen, K.; Liu, Z.; Tang, Z.; Ma, L.; et al. Phase Transition Induced Unusual Electrochemical Performance of V2CTX MXene for Aqueous Zinc Hybrid-Ion Battery. *ACS Nano* **2020**, *14*, 541−551.
(11) Li, Z.; Chen, D.; An, Y.; Chen, C.; Wu, L.; Chen, Z.; Sun, Y.; Zhang, X. Flexible and anti-freezing quasi-solid-state zinc ion hybrid supercapacitors based on pencil shavings derived porous carbon. *Energy Storage Mater.* **2020**, *28*, 307−314.
(12) Wang, H.; Yang, Y.; Guo, L. Nature-Inspired Electrochemical Energy-Storage Materials and Devices. *Adv. Energy Mater.* **2017**, *7*, No. 1601709, DOI: 10.1002/aenm.201601709.
(13) Tang, Y.; Liu, C.; Zhu, H.; Xie, X.; Gao, J.; Deng, C.; Han, M.; Liang, S.; Zhou, J. Ion-confinement effect enabled by gel electrolyte for highly reversible dendrite-free zinc metal anode. *Energy Storage Mater.* **2020**, *27*, 109−116.
(14) Zhang, X.; Pei, Z.; Wang, C.; Yuan, Z.; Wei, L.; Pan, Y.; Mahmood, A.; Shao, Q.; Chen, Y. Flexible Zinc-Ion Hybrid Fiber Capacitors with Ultrahigh Energy Density and Long Cycling Life for Wearable Electronics. *Small* **2019**, *15*, No. 1903817.
(15) Gong, J. P. Materials both Tough and Soft. *Science* **2014**, *344*, 161−162.
(16) Li, H.; Lv, T.; Li, N.; Yao, Y.; Liu, K.; Chen, T. Ultraflexible and tailorable all-solid-state supercapacitors using polyacrylamide-based hydrogel electrolyte with high ionic conductivity. *Nanoscale* **2017**, *9*, 18474−18481.
(17) Deng, W.; Zhou, Z.; Li, Y.; Zhang, M.; Yuan, X.; Hu, J.; Li, Z.; Li, C.; Li, R. High-Capacity Layered Magnesium Vanadate with Concentrated Gel Electrolyte toward High-Performance and Wide-Temperature Zinc-Ion Battery. *ACS Nano* **2020**, *14*, 15776−15785.
(18) Raj, C. J.; Varma, K. B. R. Synthesis and electrical properties of the (PVA)0.7(KI) 0.3·xH2SO4 ($0 \leq x \leq 5$) polymer electrolytes and their performance in a primary Zn/MnO2 battery. *Electrochim. Acta* **2010**, *56*, 649−656, DOI: 10.1016/j.electacta.2010.09.076.
(19) Mitha, A.; Mi, H.; Dong, W.; Cho, I. S.; Ly, J.; Yoo, S.; Bang, S.; Hoang, T. K. A.; Chen, P. Thixotropic gel electrolyte containing poly(ethylene glycol) with high zinc ion concentration for the secondary aqueous Zn/LiMn2O4 battery. *J. Electroanal. Chem.* **2019**, *836*, 1−6, DOI: 10.1016/j.jelechem.2019.01.014.
(20) Wang, Z.; Mo, F.; Ma, L.; Yang, Q.; Liang, G.; Liu, Z.; Li, H.; Li, N.; Zhang, H.; Zhi, C. Highly Compressible Cross-Linked Polyacrylamide Hydrogel-Enabled Compressible Zn−MnO2 Battery and a Flexible Battery−Sensor System. *ACS Appl. Mater. Interfaces* **2018**, *10*, 44527−44534.
(21) Cao, L.; Yang, M.; Wu, D.; Lyu, F.; Sun, Z.; Zhong, X.; Pan, H.; Liu, H.; Lu, Z. Biopolymer-chitosan based supramolecular hydrogels as solid state electrolytes for electrochemical energy storage. *Chem. Commun.* **2017**, *53*, 1615−1618.
(22) Zhang, S.; Yu, N.; Zeng, S.; Zhou, S.; Chen, M.; Di, J.; Li, Q. An adaptive and stable bio-electrolyte for rechargeable Zn-ion batteries. *J. Mater. Chem. A* **2018**, *6*, 12237−12243.
(23) Harris, J. M. *Poly(ethylene glycol) Chemistry: Biotechnical and Biomedical Applications*; Springer Science & Business Media, 1992.
(24) Oyaizu, K.; Suga, T.; Yoshimura, K.; Nishide, H. Synthesis and characterization of radical-bearing polyethers as an electrode-active material for organic secondary batteries. *Macromolecules* **2008**, *41*, 6646−6652.
(25) Schröter, E.; Elbinger, L.; Mignon, M.; Friebe, C.; Brendel, J. C.; Hager, M. D.; Schubert, U. S. High-capacity semi-organic polymer batteries: From monomer to battery in an all-aqueous process. *J. Power Sources* **2023**, *556*, No. 232293.
(26) Kardjilov, N.; Hilger, A.; Manke, I. Conrad-2: cold neutron tomography and radiography at BER II (V7). *J. Large-Scale Res. Facil. JLSRF* **2016**, *2*, No. A98, DOI: 10.17815/jlsrf-2-108.
(27) Rudin, L. I.; Osher, S.; Fatemi, E. Nonlinear total variation based noise removal algorithms. *Phys. D* **1992**, *60*, 259−268.
(28) Strong, D.; Tony, C. Edge-preserving and scale-dependent properties of total variation regularization. *Inverse Probl.* **2003**, *19*, No. S165, DOI: 10.1088/0266-5611/19/6/059.
(29) Schindelin, J.; Arganda-Carreras, E.; Frise, E.; Kaynig, V.; Longair, M.; Pietzsch, T.; Preibisch, S.; Rueden, C.; Saalfeld, S.; Schmid, B.; Tinevez, J.-Y.; et al. Fiji: an open-source platform for biological-image analysis. *Nat. Methods* **2012**, *9*, 676−682, DOI: 10.1038/nmeth.2019.
(30) Schneider, C. A.; Rasband, W. S.; Eliceiri, K. W. NIH Image to ImageJ: 25 years of image analysis. *Nat. Methods* **2012**, *9*, 671−675, DOI: 10.1038/nmeth.2089.
(31) Muench, S.; Burges, R.; Lex-Balducci, A.; Brendel, J. C.; Jäger, M.; Friebe, C.; Wild, A.; Schubert, U. S. Printable ionic liquid-based gel polymer electrolytes for solid state all-organic batteries. *Energy Storage Mater.* **2020**, *25*, 750−755.
(32) Isken, P.; Winter, M.; Passerini, S.; Lex-Balducci, A. Methacrylate based gel polymer electrolyte for lithium-ion batteries. *J. Power Sources* **2013**, *225*, 157−162.

(33) Steinhauer, W.; Keul, H.; Möller, M. Synthesis of reversible and irreversible cross-linked (M) PEG-(meth) acrylate based functional copolymers. *Polym. Chem.* **2011**, *2*, 1803−1814.
(34) Meenach, S. A.; Anderson, K. W.; Hilt, J. Z. Synthesis and characterization of thermoresponsive poly(ethylene glycol)-based hydrogels and their magnetic nanocomposites. *J. Polym. Sci., Part A: Polym. Chem.* **2010**, *48*, 3229−3235.
(35) Samchenko, Y.; Ulberg, Z.; Korotych, O. Multipurpose smart hydrogel systems. *Adv. Colloid Interface Sci.* **2011**, *168*, 247−262.
(36) Cheng, Y.; Chi, X.; Yang, J.; Liu, Y. Cost attractive hydrogel electrolyte for low temperature aqueous sodium ion batteries. *J. Energy Storage* **2021**, *40*, No. 102701.
(37) Choudhury, N. A.; Shukla, A. K.; Sampath, S.; Pitchumani, S. Cross-Linked Polymer Hydrogel Electrolytes for Electrochemical Capacitors. *J. Electrochem. Soc.* **2006**, *153*, No. A614, DOI: 10.1149/1.2164810.
(38) Márquez, I.; Paredes, N.; Alarcia, F.; Velasco, J. I. Influence of Acrylonitrile Content on the Adhesive Properties of Water-Based Acrylic Pressure-Sensitive Adhesives. *Polymer* **2022**, *14*, No. 909, DOI: 10.3390/polym14050909.
(39) Sruthi, P. R.; Anas, S. An overview of synthetic modification of nitrile group in polymers and applications. *J. Polym. Sci.* **2020**, *58*, 1039−1061.
(40) Gerlach, P.; Balducci, A. The influence of current density, rest time and electrolyte composition on the self-discharge of organic radical polymers. *Electrochim. Acta* **2021**, *377*, No. 138070.
(41) Zuo, Y.; Wang, K.; Pei, P.; Wei, M.; Liu, X.; Xiao, Y.; Zhang, P. Zinc dendrite growth and inhibition strategies. *Mater. Today Energy* **2021**, *20*, No. 100692.
(42) Chen, M.; Chen, J.; Zhou, W.; Han, X.; Yao, Y.; Wong, C. P. Realizing an All-Round Hydrogel Electrolyte toward Environmentally Adaptive Dendrite-Free Aqueous Zn−MnO2 Batteries. *Adv. Mater.* **2021**, *33*, No. 2007559, DOI: 10.1002/adma.202007559.
(43) Yan, Y.; Kong, Q.-R.; Sun, C.-C.; Yuan, J.-J.; Huang, Z.; Fang, L.-F.; Zhu, B.-K.; Song, Y.-Z. Copolymer-assisted Polypropylene Separator for Fast and Uniform Lithium Ion Transport in Lithium-ion Batteries. *Chin. J. Polym. Sci.* **2020**, *38*, 1313−1324.
(44) Lou, X.; Chen, M.; Hu, B. The effect of nitrogen and oxygen coordination: toward a stable anode for reversible lithium storage. *New J. Chem.* **2018**, *42*, 15698−15704, DOI: 10.1039/C8NJ03367F.
(45) Lin, Y.; Zhang, Q.; Zhao, C.; Li, H.; Kong, C.; Shen, C.; Chen, L. An exceptionally stable functionalized metal−organic framework for lithium storage. *Chem. Commun.* **2015**, *51*, 697−699.
(46) Yang, H.; Yin, L.; Shi, H.; He, K.; Cheng, H.-M.; Li, F. Suppressing lithium dendrite formation by slowing its desolvation kinetics. *Chem. Commun.* **2019**, *55*, 13211−13214.
(47) Kuntyi, O. I.; Zozulya, G. I. Morphology of dispersed zinc deposited by pulsed current in a ZnCl2−NH4Cl electrolyte. *Russ. J. Appl. Chem.* **2010**, *83*, 826−830.
(48) Biton, M.; Tariq, F.; Yufit, V.; Chen, Z.; Brandon, N. Integrating multi-length scale high resolution 3D imaging and modelling in the characterisation and identification of mechanical failure sites in electrochemical dendrites. *Acta Mater.* **2017**, *141*, 39−46.
(49) Hao, J.; Long, J.; Li, B.; Li, X.; Zhang, S.; Yang, F.; Zeng, X.; Yang, Z.; Pang, W. K.; Guo, Z. Toward High-Performance Hybrid Zn-Based Batteries via Deeply Understanding Their Mechanism and Using Electrolyte Additive. *Adv. Funct. Mater.* **2019**, *29*, No. 1903605.

https://doi.org/10.1021/acs.jpcc.4c00654
J. Phys. Chem. C 2024, 128, 11465−11476